Received: 17 October 2020 | Revised: 26 May 2021 | Accepted: 31 May 2021 | Accepted article online: 1 June 2021

DOI: 10.1002/prca.202000079

Proteomics Clinical Applications

RESEARCH ARTICLE

MALDI mass spectrometry imaging unravels organ and amyloid-type specific peptide signatures in pulmonary and gastrointestinal amyloidosis

Jan Schürmann[1] | Juliane Gottwald[1] | Georg Rottenaicher[2] | Andreas Tholey[3] | Christoph Röcken[1]

[1] Department of Pathology, Christian-Albrechts-University, Kiel, Germany

[2] Center for Integrated Protein Science Munich at the Department of Chemistry, Technical University of Munich, Garching, Germany

[3] Systematic Proteome Research & Bioanalytics, Institute of Experimental Medicine, Christian-Albrechts-University, Kiel, Germany

Correspondence
Christoph Röcken, Department of Pathology, Christian-Albrechts-University, Arnold-Heller-Str. 3, Building U33, D-24105 Kiel, Germany.
Email: christoph.roecken@uksh.de

Funding information
Germany Research Foundation, Grant/Award Numbers: Ro 1173/11, Ro 1173/14

Abstract

Purpose: Amyloidosis is a disease group caused by pathological aggregation and deposition of peptides in diverse tissue sites. Recently, matrix-assisted laser desorption/ionization mass spectrometry imaging coupled with ion mobility separation (MALDI-IMS MSI) was introduced as a novel tool to identify and classify amyloidosis using single sections from formalin-fixed and paraffin-embedded cardiac biopsies. Here, we tested the hypothesis that MALDI-IMS MSI can be applied to lung and gastrointestinal specimens.

Experimental Design: Forty six lung and 65 gastrointestinal biopsy and resection specimens with different types of amyloid were subjected to MALDI-IMS MSI. Ninety three specimens included tissue areas without amyloid as internal negative controls. Nine cases without amyloid served as additional negative controls.

Results: Utilizing a peptide filter method and 21 known amyloid specific tryptic peptides we confirmed the applicability of a universal peptide signature with a sensitivity of 100% and a specificity of 100% for the detection of amyloid deposits in the lung and gastrointestinal tract. Additionally, the frequencies of individual m/z-values of the 21 tryptic marker peptides showed organ- and tissue-type specific differences.

Conclusions and Clinical Relevance: MALDI-IMS MSI adds a valuable analytical approach to diagnose and classify amyloid and the detection frequency of individual tryptic peptides is organ-/tissue-type specific.

KEYWORDS
amyloidosis, formalin-fixed and paraffin-embedded, ion mobility separation, MALDI-IMS MS imaging

Abbreviations: ABC, ammonium bicarbonate; AA, amyloid A; ALκ, amyloid immunoglobulin kappa light chain; ALλ, amyloid immunoglobulin lambda light chain; ApoAI, apolipoprotein AI; ApoE, apolipoprotein E; ATTR, transthyretin amyloid; CAA, chloroacetamide; CHCA, α-cyano-4-hydroxycinnamic; DDW, double-distilled water; FFPE, formalin-fixed and paraffin-embedded; IGLC, immunoglobulin light chain constant region; IMS, ion mobility separation; LC-ESI-MS/MS, liquid chromatography electrospray ionisation mass spectrometry; LC-MS/MS, liquid chromatography tandem mass spectrometry; LMD, laser microdissection; MDIC, mass accuracy, drift time, image correlation coefficient; MS, mass spectrometry; MSI, mass spectrometry imaging; OcGlc, octyl-α/β-glucoside; SAA, serum amyloid A; SAP, serum amyloid P-component; SVM, support vector machine; TCEP, tris(2-carboxyethyl)phosphine; TFA, trifluoroacetic acid; VTN, vitronectin

1 | INTRODUCTION

Amyloidosis comprises a disease group caused by the pathological aggregation and deposition of proteins and peptides in diverse tissues and organ sites. So far, 36 proteins and peptides have been found, which are able to form amyloid, some causing devastating diseases [1,2]. Accurate diagnosis and classification are of paramount importance. Treatment options have increased for some types of amyloidosis and patient management relies on the correct classification of the amyloid type [3,4]. The diagnosis is reached by the examination of a tissue specimen using Congo red staining and polarization microscopy: amyloid shows a typical and highly specific yellow-red-green birefringence. Subsequent identification of the amyloid fibril protein and hence amyloidosis is mandatory as patient prognosis and management depend on the nature of the amyloid protein and underlying disease, for example, hereditary or acquired and localized or systemic [5].

Different approaches can be used to classify amyloid. Immunostaining of serial sections of formalin-fixed and paraffin-embedded (FFPE) tissue specimens has demonstrated its validity in specialized laboratories [6, 7]. This method provides rapid results usually within 2 days and financial costs are relatively low. Disadvantages of immunohistochemistry are the restriction to detect only known amyloid fibril proteins and the limited availability of appropriate, often laboratory-developed antibodies. However, amyloid deposits are constituted of many more non-fibrillary, although amyloid-specific constituents, which could be utilized for amyloid diagnostics. Here, the application of proteomic technologies is an alternative method and has been proven to be suitable for both, amyloid typing and identification of novel hitherto unknown amyloid fibril proteins. Laser microdissection (LMD) coupled to liquid chromatography tandem mass spectrometry (LC-MS/MS) is a valuable tool for amyloid typing [8–12]. Congo red-positive tissue areas are microdissected by a laser prior to mass spectrometry (MS) analysis, thereby avoiding contamination by serum-derived amyloidogenic proteins of adjacent unaffected tissue. The enrichment of amyloid-containing tissue achieved by LMD improved the quality of spectra compared to classical LC-MS/MS analysis of whole tissue sections and enables the classification of amyloid with high specificity and sensitivity [12,13]. In the last years there have been different studies, which reveal the possibility of using LMD LC-MS/MS to identify unknown amyloid proteins as well as glomerular proteomic profiles of various types of glomerulonephritis [14–16]. However, Congo red staining is still required to guide LMD. In addition, the loss of spatial information hampers a direct assignment of the proteins to amyloid deposits.

Recently, matrix-assisted laser desorption/ionization MS imaging (MALDI-MSI) was applied as another proteomic tool. MALDI-MSI allows the detection of both the molecular weight and the spatial distribution of a mixture of peptides and proteins in a single experiment [17–20]. It can be used to identify amyloid and amyloid-associated constituents coupled with spatial resolution [21]. In a more recent study, MALDI-MSI was used to visualize the morphological distribution of amyloidogenic as well as amyloid-associated proteins after identification by LC-MS/MS [22]. To assign the proteins to amyloid deposits the peptide images were compared with a Congo red-stained serial section. The latter was also used to guide the peptide extraction prior to LC-MS/MS analysis on a third serial section after on-tissue digestion. Furthermore, it was demonstrated that MALDI-MSI can be used for typing of amyloid A (AA) and immunoglobulin kappa light chain-associated (ALκ) amyloidosis in renal FFPE biopsies. For this purpose, spectral data of congophilic regions were selected in the MS image data and exported to build a classification model based on a support vector machine (SVM) algorithm [23].

Our group recently exploited the utility of MALDI-IMS MSI [24]. Utilizing a novel peptide filter method identified a universal peptide signature for amyloidoses. Furthermore, differences in the peptide composition of immunoglobulin lambda light chain- (ALλ) and transthyretin-associated (ATTR) amyloid were revealed and used to build a reliable classification model. We developed a bioinformatic workflow facilitating the detection and classification of amyloidosis in a single tissue section by augmenting MALDI-IMS MSI analysis with the peptide filter [24]. However, this approach was only applied to cardiac biopsies up to now. In the current study, we tested the hypothesis that MALDI-IMS MSI can also be applied to other amyloid-bearing tissue samples, that is, lung and gastrointestinal specimens.

Clinical Relevance

Amyloidosis is a disease group caused by the pathological aggregation and deposition of proteins and peptides in diverse tissues and organ sites. Prognosis and therapeutic strategies depend on the nature of the amyloid protein and the underlying disease. Accurate diagnosis and amyloid typing are of paramount importance. Previously, we developed a bioinformatics workflow for the tissue-based analysis of amyloidosis by matrix-assisted laser desorption/ionization mass spectrometry imaging coupled with ion mobility separation (MALDI-IMS MSI) using a single tissue section obtained from cardiac biopsies. Here, we extended our studies on a large patient cohort (n = 111) with pulmonary and gastrointestinal amyloidosis and independently validated the suitability of MALDI-IMS MSI to diagnose and classify amyloid at different anatomical sites. The new diagnostic tool has the advantage that the mass signature stays unaffected after MALDI measurement and the same tissue section can be used for further investigations. Our results demonstrate that MALDI-IMS MSI has the potential to diagnose and classify amyloid not only based on the amyloid protein but also on an organ- and amyloid-type specific signature of amyloid-associated constituents.

TABLE 1 Overview of the study cohort

Amyloid type	Number of cases	Lung (men/women)	Gastrointestinal tract (men/women)
ALλ amyloid	72	37 (24/13)	35 (23/12)
ALκ amyloid	22	4 (1/3)	18 (10/8)
ATTR amyloid	8	2 (2/0)	6 (3/3)
AA amyloid	4	–	4 (1/3)
AL amyloid n.o.s.	5	3 (2/1)	2 (1/1)
Total number of cases with amyloid	111	46 (29/17)	65 (38/27)
Controls without amyloid	9	3 (2/1)	6 (1/5)

Abbreviations: ATTR, transthyretin amyloid; AA, amyloid A; ALκ, amyloid immunoglobulin kappa light chain; ALλ, amyloid immunoglobulin lambda light chain.

2 | MATERIALS AND METHODS

2.1 | Patients

FFPE tissue samples obtained from 111 patients were retrieved from the Amyloid Registry of the Christian-Albrechts-University of Kiel. The presence of amyloid had been confirmed histologically for all samples by Congo red staining and polarization microscopy. The cohorts consisted of 46 lung specimens (29 men, 17 women; mean patient age 67.2 ± 10.2 years) and 65 tissue specimens (38 men, 27 women; mean patient age 69.4 ± 10.4 years) obtained from the gastrointestinal tract, that is, the stomach (56 cases [86%]), the duodenum (7 [11%]) and large intestine (2 [3%]) (Table 1). Among the cases with pulmonary AL amyloidosis, previously, 16 had been classified as a localized and five as a systemic form [25]. After the presence of amyloid was confirmed histologically, amyloid typing was done by immunohistochemistry as described in detail elsewhere [6,7,26,27]. From our lung cohort, one case of local pulmonary ALλ amyloidosis was chosen for the validation of immunoglobulin light chain constant region (IGLC) peptides.

Tissue sections from nine cases without amyloid served as a negative control (Table 1). These included three lung specimens obtained from two men and a woman (mean patient age: 42.0 ± 10.8 years), who had undergone surgery for pulmonary metastasis of rectal cancer, pulmonary adenocarcinoma and emphysema, respectively. Non-neoplastic lung tissue was used for MALDI-IMS MSI. Six specimens were obtained from the gastrointestinal tract of five women and a man (two form the stomach, four from the large intestine; mean patient age 44.5 ± 19.2 years). The gastrointestinal biopsies were obtained by endoscopy and showed normal histology. Amyloid was excluded in each negative control by Congo red staining and polarization microscopy.

Ethical approval was obtained from the local ethical review board (D 581/15-585/15). All patient data were pseudonymized after study inclusion.

2.2 | Materials

The following materials were used: trypsin (Promega; Mannheim, Germany), α-cyano-4-hydroxycinnamic acid (CHCA; LaserBio Labs, Sophia-Antipolis Cedex, France), double-distilled water (DDW, Carl Roth, Karlsruhe, Germany), xylene (BüFa, Lübeck, Germany), acetonitrile and ethanol (both Merck, Darmstadt, Germany), trifluoroacetic acid (TFA), tris(2-carboxyethyl)phosphine (TCEP), chloroacetamide (CAA), ammonium bicarbonate (ABC), octyl-α/β-glucoside (OcGlc), red phosphorous, and acetone (all Sigma Aldrich, Steinheim, Germany).

2.3 | Sample preparation

MALDI-IMS MSI sample preparation was done as previously described [24]. In brief, 2 μm thick paraffin sections were cut with a microtome (Leica Biosystems, Nussloch, Germany), placed onto a histological glass slide (up to three tissue sections per slide; SuperFrost® Plus, Menzel-Gläser, Thermo-Fisher Scientific, Schwerte, Germany) and dried overnight at 54°C. Paraffin was removed by xylene (dewaxing; 2 × 15 min), followed by rehydration in a descending ethanol series (99%, 70%, and 50%, each 2 × 2 min) and double distilled water (DDW, 2 × 1 min). Antigen retrieval was performed in citric acid buffer (10 mM, pH 6.0) at 100°C for 30 min using a pressure cooker (Pascal S2800, DakoCytomation, California, Inc., USA). The sections were cooled down in a water bath at 10°C for 15 min, rinsed 10 times with DDW and dried in a desiccator at room temperature under a vacuum of −800 mBar for at least 15 min. On-tissue digestion was carried out by spraying 10 layers of a trypsin solution (0.05 μg/μL in 50 mM NH_4HCO_3 with water/10 % ACN:OcGlc, 99.5:0.5, v/v, pH 8.1) with a constant flow rate (10 μL/min) onto the tissue section utilizing the SunCollect Micro Fraction Collector/MALDI Spotter (SunChrom, Friedrichsdorf, Germany) followed by incubation for 2 h at 37°C in an in-house humidity chamber. CHCA matrix solution (5 mg/mL in water/0.2 % TFA:ACN, 50:50, v/v) was applied over nine layers with an increasing flow rate for the first four layers (1st at 20 μL/min, 2nd at 30 μL/min, 3rd at 40 μL/min and 4th–8th at 50 μL/min) resulting in a homogeneous crystallization.

For MALDI-IMS MS/MS, a pulmonary FFPE tissue sample was cut to 10 μm thick sections, placed onto histological glass slides and dewaxed by immersing into xylene for 10 min, followed by re-hydration with 99% ethanol for 10 min. Subsequently ~0.3 mmş tissue was scraped off and transferred to a reaction tube, lyophilized (Scanvac Coolsafe, LaboGene, Allerød, Denmark), and stored at −80°C until further usage.

For peptide extraction the SPEED protocol was applied [28]. Ten microliter TFA were added to each sample, incubated for 10 min, and neutralized with 100 μL Tris (2 M). Proteins were reduced by adding 11 μL TCEP (100 mM) at 95°C for 30 min, followed by alkylation with 11 μL CAA (400 mM) at 21°C room temperature for 20 min. Tissue extracts were diluted with 610 μL water, digested by adding 10 μL trypsin (0.1 μg/ μL) in ABC-buffer (50 mM), and incubated at 37°C and 600 rpm for 20 h (Eppendorf ThermoMixer C, Hamburg, Germany). Extracts were lyophilized, dissolved in 100 μL 0.1% TFA (v/v), and desalted using C18 tips (Pierce C18 tips 100 μL, Pierce Biotechnology, Rockford, USA) according to the manufacturer's instructions. Subsequently samples were eluted with 10 μL 90% acetonitrile and 0.1% TFA (v/v), dried in a vacuum centrifuge (Eppendorf Concentrator plus, Hamburg, Germany), and reconstituted in 20 μL 3% acetonitrile and 0.1% TFA (v/v).

The recombinant light chain FOR005 refers to the light chain of an ALλ amyloidosis case with cardiac involvement. Recombinant light chain FOR005 was expressed and purified as previously described [29]. Briefly, the DNA plasmid (pET28b) encoding for FOR005 light chain was transformed into *Escherichia coli* BL21 (DE3)-star cells and the protein was expressed as insoluble inclusion bodies over night at 37°C using 1 mmol/L isopropyl β-D-1-thiogalactopyranosid for induction. After harvesting, cell disruption, and centrifugation, inclusion bodies were solubilized in 50 mM Tris/HCl, 8 M urea, 0.1 % β-mercaptoethanol, and pH 8.0 at room temperature for 4–8 h. Subsequently, dialysis against an excess of 50 mM Tris, 5 M urea, pH 8.0 was performed at 10°C over night. Afterwards, anion exchange chromatography using Q-Sepharose (GE Healthcare, Uppsala, Sweden) was carried out and protein-containing fractions were pooled and diluted to 0.5 mg/mL protein or below. The diluted protein solution was then dialyzed against an excess of 50 mM Tris, 3 M urea, pH 8.5 at 10°C over night. Afterwards, the protein was dialyzed against phosphate buffered saline pH 7.4 for approximately 24 h at 10°C. As a polishing step, the refolded protein was concentrated and purified by size exclusion chromatography using a Superdex75 column (GE Healthcare, Uppsala, Sweden) running in phosphate buffered saline pH 7.4. For in-solution digest 10 μg recombinant FOR005 light chain were dissolved in 20 μL ammonium bicarbonate ABC-buffer (50 mM), reduced with 2 μL TCEP (100 mM), alkylated with 2 μL CAA (400 mM), and digested by adding 5 μL trypsin (0.1 μg/ μL). Sample volume was adjusted to 100 μL with 0.1% TFA (v/v) and peptides were desalted, followed by elution with 10 μL of 90% acetonitrile and 0.1% TFA.

2.4 | MALDI-IMS MS imaging

Imaging experiments were performed using the MALDI SYNAPT G2-S (Waters Corporation, Manchester, U.K.) equipped with a 1 kHz Nd:YAG laser operating in positive ion V-mode as described previously [24]. External calibration of the mass spectrometer was carried out using signals of red phosphorous. Imaging measurements were performed for all cases with ion mobility separation in the mass range from 700 to 2000 m/z at a spatial resolution of 200 μm and 1000 laser shots (1 s) per position. The IMS parameters trap bias DC, wave velocity (WV) and transfer wave velocity (TWV) were set at 70 V, 350 and 175 m/s, respectively. Regions for acquisition were defined with the High Definition Imaging software (HDI) (v1.3.5, Waters) on imported digital scans (Epson Perfection 1640SU; Seiko Epson Corporation, Meerbusch, Germany) of the tissue sections. Peptide images were generated with the Apex3D algorithm (m/z window: 0.1 Da, intensity threshold: 10 counts; drift window: 5 bins; IMS peak width: 2–10 bins) for the 3000 most intense signals and visualized with the HDI software. The spectral data were normalized against the base peak and recalibrated with an external lock mass (CHCA matrix cluster signal at m/z 825.101). For the detection of 21 tryptic peptides derived from apolipoprotein AI (ApoAI), apolipoprotein E (ApoE), serum amyloid A (SAA), serum amyloid P-component (SAP), transthyretin (TTR), vitronectin (VTN), and two IGLC peptides ($IGLC_1$ and $IGLC_2$) the processed imaging data were filtered by mass accuracy, drift time, and image correlation coefficient with tolerances set at 30 ppm (lung) and 40 ppm (gastrointestinal), 2.5 bins and 0.75–1.00, respectively. Previously, the ApoE m/z 968.55 was identified in 62 of the 66 heart tissue samples (94%) [24]. In our current series, it was found in every case and always matched the Congo red-stained amyloid deposits (Table 2). Therefore, the peptide image of 968.55 m/z was used as reference image to determine the Pearson correlation coefficient (R) for the other peptide images utilizing the HDI software. Peptide masses fulfilling all three criteria were considered as detected and identified.

To add potential tryptic ALλ peptides to our peptide filter we analyzed $IGLC_{1/2}$ MS/MS spectra and determined their drift time in ion mobility. The tryptic digest and the peptides derived from the SPEED-extraction from pulmonary tissues were analyzed by MALDI-IMS MS/MS as reported earlier [24]; additionally, the pulmonary sample was also analyzed by LC-ESI MS/MS (Method S1). To add newly identified light chain peptides to our pre-existing peptide target filter the drift time for each peptide was averaged from $n = 4$ recombinant light chain and $n = 2$ lung sample measurements by MALDI-IMS MS using DriftScope v2.9 (Waters Corporation, Manchester, UK).

2.5 | Statistics

All imaging data were reprocessed as described above but with an additional target list consisting of the 21 theoretical peptide masses from ApoAI, ApoE, SAA, SAP, TTR, VTN, and $IGLC_{1/2}$, as well as their specific drift times. Spectral data of regions showing high signal intensities of the peptide mass at m/z 968.55 were normalized against the total ion current and exported for statistical analysis using the HDI software. SPSS version 25 (IBM Corp., Armonk, NY, USA) was used for statistical analyzes. The Fischert's exact test was used for testing significant differences between AL amyloidosis of the lung and the gastrointestinal tract. We assumed a significance level of $p = 0.05$. All p-values are shown uncorrected. To compensate for the false discovery rate (FDR) within the correlations, we applied the Simes (Benjamini-Hochberg) procedure (FDR correction) [30]. In this study 15 out of 21 p-values showed significant levels and no p-values below 0.05% were dropped out.

TABLE 2 Detection frequencies of m/z values in pulmonary and gastrointestinal amyloid deposits of all cases ($n = 46$ and $n = 65$) and of the cases with AL amyloidosis ($n = 41$ and $n = 53$)

Protein	m/z	All cases				AL amyloidosis				
		Lung		Gastrointestinal		Lung		Gastrointestinal		*p*-value[a]
		n_D/n_A	(%)	n_D/n_A	(%)	n_D/n_A	(%)	n_D/n_A	(%)	
ApoE	948.52	38/46	(83)	26/65	(40)	35/41	(85)	22/53	(42)	0.000
	968.55	46/46	(100)	65/65	(100)	41/41	(100)	53/53	(100)	Nc
	1497.80	29/46	(63)	33/65	(51)	25/41	(61)	28/53	(53)	0.530
SAP	764.44	31/46	(67)	29/65	(45)	29/41	(71)	24/53	(45)	0.021
	1156.59	7/46	(15)	0/65	(0)	7/41	(17)	0/53	(0)	0.002
	1406.66	29/46	(63)	63/65	(97)	26/41	(63)	52/53	(98)	0.000
	1811.89	27/46	(59)	52/65	(80)	26/41	(63)	42/53	(79)	0.107
VTN	887.50	25/46	(54)	56/65	(86)	22/41	(54)	47/53	(89)	0.000
	1314.68	27/46	(59)	55/65	(85)	24/41	(59)	44/53	(83)	0.011
	1422.65	32/46	(70)	57/65	(88)	29/41	(71)	48/53	(91)	0.016
	1503.83	9/46	(20)	3/65	(5)	8/41	(20)	2/53	(4)	0.019
	1646.81	8/46	(17)	54/65	(83)	7/41	(17)	45/53	(85)	0.000
	1666.77	30/46	(65)	58/65	(89)	25/41	(61)	50/53	(94)	0.000
ApoA1	781.43	35/46	(76)	27/65	(42)	31/41	(76)	23/53	(43)	0.003
	1031.51	42/46	(91)	58/65	(89)	37/41	(90)	47/53	(89)	1.000
	1301.64	43/46	(93)	59/65	(91)	38/41	(93)	48/53	(91)	1.000
SAA	1612.81	10/46	(22)	34/65	(52)	8/41	(20)	30/53	(57)	0.000
	1670.79	9/46	(20)	34/65	(52)	9/41	(22)	29/53	(55)	0.002
TTR	1366.75	14/46	(30)	4/65	(6)	12/41	(29)	2/53	(4)	0.001
$IGLC_1$	1743.86	19/46	(41)	2/65	(3)	16/41	(39)	2/53	(4)	0.000
$IGLC_2$	1986.02	0/46	(0)	1/65	(2)	0/41	(0)	1/53	(2)	1.000

Statistical testing with Fisher-test was done to reveal significant organ-specific differences in AL amyloidosis

Abbreviations: ApoE, apolipoprotein E; ApoAI, apolipoprotein AI; SAP, serum amyloid P-component; SAA, serum amyloid A; VTN, vitronectin; TTR, transthyretin; IGLC, immunoglobulin light chain constant region.

[a] Fisher's exact test.

3 | RESULTS

Previously, we have shown that 19 tryptic peptides derived from ApoAI, ApoE, SAA, SAP, TTR, and VTN identified by MALDI MS/MS are spatially enriched in cardiac amyloid deposits [24]. In the first set of experiments, we tested the hypothesis that the specific spatial enrichment and co-localization of these 19 tryptic peptides (Table 2) also applies to amyloid deposits of extracardiac tissues, that is, the lung and gastrointestinal tract. Additionally, we added two tryptic IGLC peptides, that is, $IGLC_1$ and $IGLC_2$, commonly observed in ALλ deposits to our filter (Gottwald and Röcken, accepted) to supplement our peptide profiling strategy: m/z 1743.8588 $[M+H]^+$ and m/z 1986.0178 $[M+H]^+$ (Figure S1). Both peptides were observed in a tryptic digest of the recombinant protein and are proteotypic. These peptides were also identified by MALDI-IMS MS and MS/MS in a case of pulmonary ALλ amyloidosis and were further confirmed by LC-ESI MS/MS (for peptide spectrum at m/z 1986.0178, see Figure S2).

Both peptides were then added to the peptide filter: m/z 1743.8588 $[M+H]^+$ with an average drift time of 139.86 bins ($n = 6$) and m/z 1986.0178 $[M+H]^+$ with 161.62 bins ($n = 6$, Table 2).

A cohort of 46 lung and 65 gastrointestinal tissue specimens was retrieved from the Amyloid Registry Kiel and tissue sections were forwarded to MALDI-IMS MSI analysis. Seventy-two cases had ALλ amyloid, 22 ALκ, 8 ATTR, 4 AA, five were classified as AL amyloid not otherwise specified (n.o.s.) (Table 1). The tryptic peptide m/z 968.55 (ApoE) was used as a reference image as it was found for all cases (also in lung and gastrointestinal specimens) and with a high abundance. None of the nine negative controls showed the reference m/z 968.55. As an additional control, co-localization of the individual tryptic peptides (= m/z images) with amyloid was confirmed by Congo red staining and polarization microscopy for each tissue section used for MALDI-IMS MSI analysis after washing off the matrix with 80% ethanol. No amyloid was found in the negative controls.

Figure 1 shows examples of pulmonary and gastrointestinal AL amyloidosis correlating m/z images with histology. The distribution of m/z 968.55 (ApoE), m/z 948.56 (ApoE), and m/z 1031.51 (ApoA1) masses analyzed by MALDI-IMS MSI correlated spatially with the

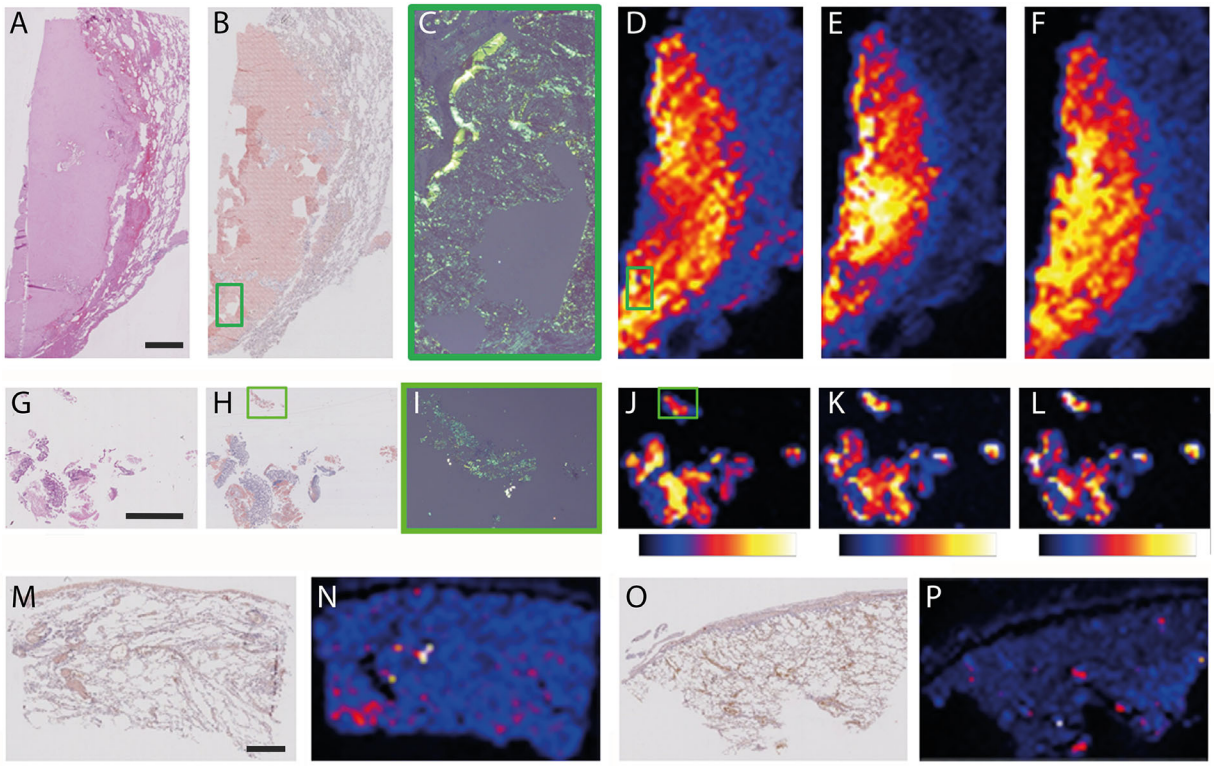

FIGURE 1 Comparison of immunohistochemical with Congo red staining after imaging measurement in pulmonary (A-F) and gastrointestinal amyloid deposits (G-L). In hematoxylin and eosin-stained sections (A, G), amyloid shows homogenous eosinophilic masses. Congo red stains the deposits reddish (B, H; bright field). Small green-framed cutout shows the same Congo red-stained tissue sections under polarized light with a typical green-yellow-red birefringence (C; I). MALDI-MS images with the same resolution as A, B, G, and H display the spatial distribution of tryptic peptides belonging to masses of ApoE (D/J = m/z 968.55, E/K = m/z 948.52) and ApoA1 (F/L = m/z 1031.51) [amyloid positive areas: yellow = high intensity; tissue areas without amyloid: blue = low intensity]. Negative controls of lung tissue without amyloid (M-P): Congo red staining illustrates the absence of amyloid (M, O; bright field) and the associated MALDI-MS images for the VTN mass of m/z 1314.65 (N/P). The spatial resolution for the peptide images is 200 μm. Scale bar 2 mm

amyloid deposits (Figure 1). High intensities of the VTN mass m/z 1314.65 that are characteristic for amyloid deposits were absent in the negative controls (Figure 1). Furthermore, Figure 1 depicts amyloid positive areas (yellow = high intensity) adjacent to tissue areas without amyloid (blue = low intensity). Tissue areas without amyloid served as an internal negative control and were present in 55 (85%) gastrointestinal and 38 (83%) lung specimens. Finally, we were able to demonstrate that all 19 tryptic peptides proposed by Winter et al. [24] and the two additional IGLC peptides correlated spatially with amyloid deposits of the lung and gastrointestinal tract, albeit with variable frequencies (Table 2).

Winter et al. [24] designed a peptide filter (MDIC) including the three parameters: (1) mass accuracy (M), (2) drift time (D) and (3) image correlation coefficient (IC), which enables a targeted detection of tryptic peptides in amyloid deposits based on MALDI-IMS MSI data. Applying this MDIC peptide filter on the processed imaging data of both cohorts, the peptides were found with a mass error of 30 ppm (lung) and 40 ppm (gastrointestinal) but not in a single case without amyloid (negative control). Slightly higher tolerances in gastrointestinal samples had to be chosen because in 13 out of 65 tissue samples the mass accuracy ranged between 33 and 35 ppm to the lower cut off. This was necessary due to a small but systematic increase of mass shifts over longer analysis times observed in our experimental setup. When all 21 tryptic peptides were utilized, the sensitivity and specificity was 100%, respectively, for the detection of amyloid deposits in pulmonary and gastrointestinal tissue specimens. In general, these data confirm the applicability of the 21 tryptic peptides and the MDIC filter to other organ and tissue types affected by amyloid.

AL amyloidosis can appear as a systemic and a local form. While systemic AL amyloidosis may need hemato-oncological care, the localized form can be treated with a more restrained approach [25]. Sixteen cases of pulmonary AL amyloid had been classified as a localized form and five as part of a systemic disease. Regarding the MDIC, no difference was found between local and systemic pulmonary AL amyloidosis (see Table S1).

Since we noticed differences in the frequencies of the individual m/z-values we next tested the hypothesis that mass spectra show organ- or tissue-type specific differences. Using the Fisher test we compared pulmonary with gastrointestinal AL amyloidosis. As summarized in Table 2, the frequencies of 15 m/z-values differed significantly between pulmonary and gastrointestinal AL amyloidosis ($p < 0.05$; Table 2). These results lead to the conjecture that mass spectra could be organ and amyloid-type specific. These differences were found for

TABLE 3 Colored overview of the detection frequencies of the 21 amyloid peptides from seven amyloid proteins of the study cohort with ALλ ($n = 72$) and ATTR ($n = 8$) amyloidosis in the lung (L) and the gastrointestinal tract (G)

Protein	Organ m/z	ALλ L [%]	ALλ G [%]	ATTR L [%]	ATTR G [%]
ApoE	948.52				
	968.55				
	1497.80				
	764.44				
SAP	1156.59				
	1406.66				
	1811.89				
VTN	887.50				
	1314.68				
	1422.65				
	1503.83				
	1646.81				
	1666.77				
ApoA1	781.43				
	1031.51				
	1301.64				
SAA	1612.81				
	1670.79				
TTR	1366.75				
$IGLC_1$	1743.86				
$IGLC_2$	1986.02				

The MALDI score serves for the colored encoding of the detection frequencies (green: 100–76%, yellow: 75–51%, orange: 50–26% and red: 25–0%)
Abbreviations: ATTR, transthyretin amyloidosis; MALDI, matrix-assisted laser desorption/ionization; ApoE, apolipoprotein E; ApoA1, apolipoprotein A1; SAP, serum amyloid P-component; SAA, serum amyloid A; VTN, vitronectin; TTR, transthyretin; IGLC, immunoglobulin light chain constant region.

all analyzed amyloid associated/amyloidogenic proteins, that is, ApoAI, ApoE, VTN, SAP, SAA, ATTR, and $IGLC_{1/2}$.

To further test this hypothesis, we visualized the differences using a MALDI score (Table 3). The MALDI score translates the detection frequencies of the most common amyloid types ALλ and ATTR for both lung and gastrointestinal amyloidosis into a color code. Table 3 illustrates the detection maxima (green) for ApoE and ApoA1 fragments in pulmonary ALλ amyloidosis, while VTN is more prevalent in gastrointestinal ALλ amyloidosis. Interestingly, no single protein stood out in pulmonary and gastrointestinal ATTR amyloidosis, although organ-type specific differences were noted on single peptide levels (e.g., m/z 1314.68 or m/z 781.43). However, Table 3 illustrates nicely amyloid-type specific differences.

Next, we assessed the suitability of IGLC to diagnose and classify amyloid. We searched the UniProt database for IGLC amino acid sequences, some of which were found repeatedly via LMD LC-MS/MS in amyloid deposits (Gottwald and Röcken, accepted) [32–36]. Reference masses were generated by in silico digest of the IGLC proteins using PeptideMass (www.expasy.org). Two unique peptide masses were found corresponding to tryptic digests of IGLC 1, 2, 3, 6, 7, and IGLC 2, 3, 6, 7 ($IGLC_1$ and $IGLC_2$, respectively; Table 2). Our cohort was then evaluated regarding the detection frequencies dependent on mass accuracy and image correlation coefficient. Differences between the two tissue types were found for m/z 1743.86.74 ($IGLC_1$) and m/z 1986.02 ($IGLC_2$). The detection frequencies of these two peptides were also different regarding AL- and ATTR amyloid (Table 3).

Finally, we were interested in the assignment of the m/z-values to the peptides. Figure 2 illustrates the distribution of the peptides representing the individual m/z-values along the full-length proteins. For example, the m/z 968.55 represents amino acid position 199 to 207 of ApoE (Figure 2). Finally, we were able to demonstrate that the detection frequencies of the individual m/z values (= tryptic peptides) is not random: the five different m/z values of VTN (framed in red) cover almost the entire length of the protein in gastrointestinal AL amyloidosis, while in gastrointestinal ATTR amyloidosis VTN peptides were localized predominantly close to the N-terminus.

4 | DISCUSSION

MALDI-IMS MSI is a new tool for the diagnosis and classification of amyloid in FFPE tissue sections. So far, it was only applied to cardiac biopsies [24]. In this study, we extended our analyzes and were able to demonstrate the applicability of MALDI-IMS MSI and the MDIC filter to amyloid containing tissue specimens obtained from the lung and gastrointestinal tract: Capturing individual images of 21 tryptic peptides by MALDI-IMS MSI confirmed their specific and spatial enrichment and co-localization with amyloid deposits at the respective organ and tissue sites (Figure 1). Interestingly, adapting the MDIC filter to the total imaging data of 111 patient samples unraveled amyloid type-specific differences in the detection frequencies of the tryptic peptides derived from seven amyloid-specific proteins, that is, ApoAI, ApoE, SAA, SAP, TTR, VTN, and IGLC (Table 2). These findings support the contention of an amyloid-specific protein/peptide signature beyond the fibril-forming amyloid protein [13]. This mixture also contains an organ-specific signature, which was visualized by the MALDI score (Table 3) and could be aligned to the protein sequences (Figure 2). Collectively, these data demonstrate that amyloid deposits contain a fibril protein and an organ-and amyloid-type specific mixture of spatially enriched proteins and peptides, which can be used to diagnose and possibly to classify amyloid using a single tissue specimen.

Currently, little is known about the origin and pathophysiological significance of the non-fibrillar components of amyloid. Using two-dimensional liquid chromatography coupled to tandem mass spectrometry (2DC—MS/MS) and a shotgun proteomics approach, Brambilla et al. identified 330 proteins observed only in amyloid containing fat tissue specimens [37]. These included membrane proteins (27%), secreted proteins (18%), and extracellular matrix (ECM)

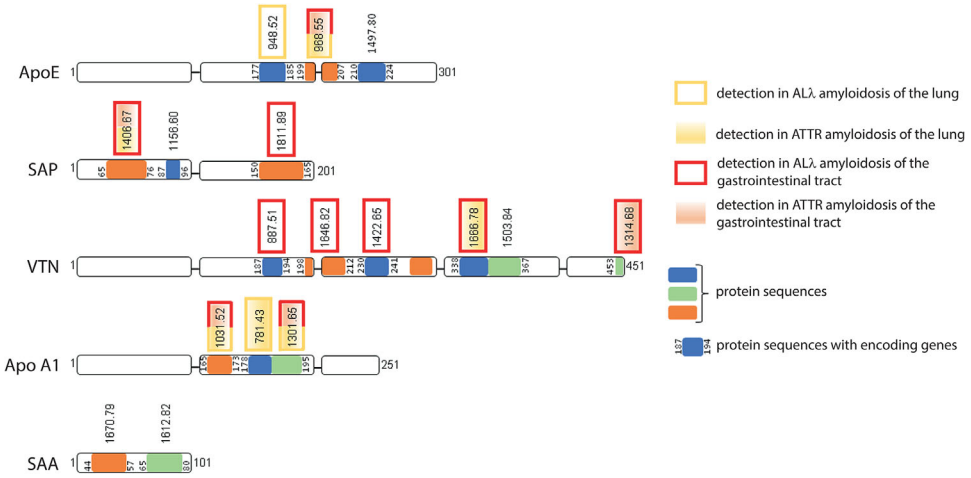

FIGURE 2 Alignment of 17 of 19 tryptic peptides along the protein sequences of their corresponding proteins

proteins (about 7%). Thus, the origin of non-fibrillar, amyloid-associated proteins and peptides is diverse. They may be present (1) locally before amyloid formation, (2) they could be products of a local cellular response to amyloid formation, (3) remnants of cell death or (4) entrapment/enrichment by non-specific and specific interactions with the amyloid precursor proteins or amyloid fibrils.

Several non-fibrillar constituents, most notably members of the ECM, might be physiological components of the local tissue environment and present before amyloid formation. Particularly, SAP is present in elastic fibers of both the lung and gastrointestinal tract. However, detection of SAP in amyloid deposits is an amyloid-specific phenomenon and due to local enrichment beyond physiological amounts and distributions. Brambilla et al. found evidence of a profound remodeling of the ECM in amyloid deposits, for example, an increase in collagen and heparan sulfate proteoglycan and a decrease in laminin and keratan sulfate [37]. Amyloid formation is dynamic and members of the local physiological tissue proteome may be still present and detectable although with lower amounts [37].

MALDI-IMS MSI could also detect remnants of preceding changes in the local environment, before amyloid formation takes place. In systemic AA amyloidosis, Claus et al. were able to show the local enrichment of amyloidogenic proteins into the interstitial matrix. The fibril-forming precursor proteins were present before amyloid formation took place [38].

Amyloid and oligomeric prefibrillar intermediates exert diverse effects on cell- and tissue homeostasis, including ECM formation, metabolic changes, cell toxicity and cell death [37,39,40]. Amyloidosis leads to remodeling of the ECM, which explains the differential expression, that is up- and down-regulation of ECM proteins, as mentioned above, and the amyloid-associated deposition of VTN [21]. Alterations of proteins involved in protein folding, lipid metabolism, glycolysis, and mitochondrial function could lead to local enrichment of, for example, apolipoproteins such as ApoE and clusterin. Clusterin is a chaperone and well-known for its interaction with amyloid deposits and proteins like ApoE, SAP or VTN [41–44]. There is also ample evidence that oligomeric prefibrillar intermediates, rather than the amyloid fibrils, are the primary cause of toxicity and cell death. Some non-fibrillar constituents of the amyloid proteome could be remnants of cell death or caused by membrane leakage, for example, by amyloidogenic oligomers forming annular channels/pores in cell membranes [45,46]. This would lead to the enrichment of proteins, which are normally not present in the extracellular space.

Post-translational modifications such as phosphorylation, proteolytic cleavage, nitration, and ubiquitination play central roles in the pathology of amyloidosis [39]. These could affect the fibril protein, but may also apply to non-fibrillar constituents [39]: the alignment of our m/z values with protein sequences showed amyloid type specific differences for VTN. Future studies should consider the possibility that proteolysis is not restricted to fibril proteins.

Interestingly, we also detected precursor proteins of other types of amyloid, for example, SAA and TTR in AL amyloidosis. This could be the result of stimulating the aggregation of one amyloid protein/peptide by another, which is called cross-seeding or heterologous seeding [39]. This could lead to the formation of fibrils consisting of more than one fibril-protein and might be a far more common phenomenon than previously expected [39,47].

A "passive" local entrapment of non-fibrillar peptides and proteins is also a possible source of amyloid-associated proteins. Amyloid deposits create mechanical barriers around cells- and close-by blood vessels and cause tissue damage [48].

All these putative mechanisms, which depend on the nature of the underlying amyloid disease (AA- vs. AL- vs. ATTR amyloidosis) and the tissue environment, ultimately might explain a disease- and tissue-type specific proteomic signature, which can be utilized for diagnostic purposes.

MALDI-IMS MSI allows the investigation of the complex, disease specific and dynamic proteome of amyloids, and offers several advantages [24]. The MDIC peptide filter allows a targeted identification of tryptic peptides in amyloid based on MALDI-IMS MS imaging data. In routine diagnostics, MS/MS analysis is not required anymore. Amyloid can be identified and diagnosed in its histoanatomical context using a universal as well as disease and organ specific peptide signature. The

integrity of the tissue specimen is preserved. The spatial distribution of amyloid can be readily visualized by the peptide mass at m/z 968.55. This allows a direct export of the spectral data of amyloid deposits for statistical analysis without additional analytical steps, for example, Congo red staining of a serial section. Due to the fact that a disease specific enrichment of peptides will result in peptide images similar to the image of m/z 968.55, the image correlation coefficient can be utilized for an untargeted screening of the imaging data to discover new potential biomarkers of amyloids. Novel biomarkers should be identified by MS/MS analysis. However, thereafter they can be added to the peptide filter's target list and improve diagnostics, as further demonstrated in this study. We were able to extend the applicability of MALDI-IMS MSI to lung and gastrointestinal specimens and validated its utility in a large and independent case series of 111 specimens. However, resolution still is an issue and tiny deposits, often encountered in biopsy specimens, can be an obstacle to MALDI-IMS MSI analytics. In addition, acquiring peptide images with higher spatial resolution might allow the detection of heterogenous composition patterns within the amyloid plaques, thus enabling a more detailed examination of the tissue remodeling processes during amyloid accumulation.

In conclusion, we could show that the MALDI-IMS MSI is an innovative tool to detect and classify various types of amyloidosis. We were able to extend the number of organs showing a specific protein signature to lung and gastrointestinal tissue, extending our experience hitherto collected only in cardiac biopsies [24]. The new diagnostic tool has the advantage that the mass signature stays unaffected after MALDI measurement and the same tissue sections can be used for further investigations. Our results show that MALDI-IMS MSI can be applied to other organ and tissue sites, carries the potential to classify amyloid not only based on the amyloid protein, but also on an organ and amyloid type specific signature of amyloid-associated constituents. However, spatial resolution is still a limitation of MALDI-IMS and further technical improvements are urgently needed.

5 | STUDY LIMITATIONS

Our MALDI-IMS MSI application does not focus on the detection of the amyloid fibril protein, but on an amyloid- and organ-type specific protein and peptide signature. AL amyloid mainly consists of the variable, joined, and only part of the constant light chain region [49]. Hence, as variable light chains are extremely variable and highly patient-specific, we have chosen IGLC for our targeted approach to detect proteins typical for AL deposits in tissue samples. Furthermore, the number of cleavage sites for trypsin digestion is structure dependent and can be affected by modifications of the amyloid forming protein [50]. Despite these challenges we clearly show the potential for direct classification of amyloid by MALDI-IMS MSI by including disease-specific, non-fibrillar constituents.

ACKNOWLEDGMENTS

The authors thank Jan Leipert for his help in setting up the mass spectrometer, Christian Treitz for his support in protein extraction prior to MALDI-IMS MS/MS analysis, and Tomas Koudelka for conducting the LC-ESI MS/MS experiment and data analysis. Moreover, we thank Hans-Michael Behrens for his help in the statistical analysis and Alex Muck (Waters, Eschborn) for his support in setting up the MALDI-IMS MS/MS method. This study was supported by grants of the German Research Foundation (Grant-No. Ro 1173/11 and Ro 1173/14). Andreas Tholey was supported by the Cluster of Excellence "Precision Medicine in Inflammation (RTF-V)".

CONFLICT OF INTEREST STATEMENT

The authors declare no competing financial interest.

AUTHOR CONTRIBUTIONS

Study concept and design were done by Jan Schürmann, Andreas Tholey, and Christoph Röcken. Surgical pathological data was obtained by Christoph Röcken and mass spectra data by Jan Schürmann, Juliane Gottwald, and Andreas Tholey. The data were analyzed and interpreted by Jan Schürmann, Juliane Gottwald, Andreas Tholey, and Christoph Röcken. Light-chain synthesis was done by Georg Rottenaicher. Drafting of the manuscript and critical revision of the manuscript for important intellectual content was done by all authors. Christoph Röcken obtained funding. Administrative, technical, or material support was provided by Andreas Tholey and Christoph Röcken. The study was supervised by Andreas Tholey and Christoph Röcken.

DATA AVAILABILITY STATEMENT

The MS proteomics data were deposited to the ProteomeXchange Consortium via PRIDE [31] partner repository with the dataset identifier PXD023813.

ORCID

Andreas Tholey https://orcid.org/0000-0002-8687-6817
Christoph Röcken https://orcid.org/0000-0002-6989-8002

REFERENCES

1. Benson, M. D., Buxbaum, J. N., Eisenberg, D. S., Merlini, G., Saraiva, M. J. M., Sekijima, Y., Sipe, J. D., & Westermark, P. (2020). Amyloid nomenclature 2020: Update and recommendations by the International Society of Amyloidosis (ISA) nomenclature committee. *Amyloid*, *27*(4), 217–222. https://doi.org/10.1080/13506129.2020.1835263
2. Chiti, F., & Dobson, C. M. (2017). Protein misfolding, amyloid formation, and human disease: A summary of progress over the last decade. *Annual Review of Biochemistry*, *86*, 27–68. https://doi.org/10.1146/annurev-biochem-061516-045115
3. Buxbaum, J. N. (2019). Treatment of hereditary and acquired forms of transthyretin amyloidosis in the era of personalized medicine: The role of randomized controlled trials. *Amyloid*, *26*(2), 55–65. https://doi.org/10.1080/13506129.2019.1575201
4. Gertz, M. A. (2020). Immunoglobulin light chain amyloidosis: 2020 update on diagnosis, prognosis, and treatment. *American Journal of Hematology*, *95*(7), 848–860. https://doi.org/10.1002/ajh.25819
5. Mahmood, S., Bridoux, F., Venner, C. P., Sachchithanantham, S., Gilbertson, J. A., Rowczenio, D., Wagner, T., Sayed, R., Patel, K., Fontana, M., Whelan, C. J., Lachmann, H. J., Hawkins, P. N., Gillmore, J. D., & Wechalekar, A. D. (2015). Natural history and outcomes in localised immunoglobulin light-chain amyloidosis: A long-term observational

study. *The Lancet Haematology*, *2*(6), e241–e250. https://doi.org/10.1016/S2352-3026(15)00068-X

6. Kebbel, A., & Röcken, C. (2006). Immunohistochemical classification of amyloid in surgical pathology revisited. *American Journal of Surgical Pathology*, *30*(6), 673–683. https://doi.org/10.1097/00000478-200606000-00002
7. Schönland, S. O., Hegenbart, U., Bochtler, T., Mangatter, A., Hansberg, M., Ho, A. D., Lohse, P., & Röcken, C. (2012). Immunohistochemistry in the classification of systemic forms of amyloidosis: A systematic investigation of 117 patients. *Blood*, *119*(2), 488–493. doi: blood-2011-06-358507 [pii];10.1182/blood-2011-06-358507 [doi] https://doi.org/10.1182/blood-2011-06-358507
8. Klein, C. J., Vrana, J. A., Theis, J. D., Dyck, P. J., Dyck, P. J. B., Spinner, R. J., Mauermann, M. L., Bergen, H. R., Zeldenrust, S. R., & Dogan, A. (2011). Mass spectrometric-based proteomic analysis of amyloid neuropathy type in nerve tissue. *Archives of Neurology*, *68*(2), 195–199. https://doi.org/10.1001/archneurol.2010.261
9. Nasr, S. H., Said, S. M., Valeri, A. M., Sethi, S., Fidler, M. E., Cornell, L. D., Gertz, M. A., Dispenzieri, A., Buadi, F. K., Vrana, J. A., Theis, J. D., Dogan, A., & Leung, N. (2013). The diagnosis and characteristics of renal heavy-chain and heavy/light-chain amyloidosis and their comparison with renal light-chain amyloidosis. *Kidney International*, *83*(3), 463–470. https://doi.org/10.1038/ki.2012.414
10. Said, S. M., Reynolds, C., Jimenez, R. E., Chen, B., Vrana, J. A., Theis, J. D., Dogan, A., & Shah, S. S. (2013). Amyloidosis of the breast: Predominantly AL type and over half have concurrent breast hematologic disorders. *Modern Pathology*, *26*(2), 232–238. https://doi.org/10.1038/modpathol.2012.167
11. Sethi, S., Vrana, J. A., Theis, J. D., Leung, N., Sethi, A., Nasr, S. H., Fervenza, F. C., Cornell, L. D., Fidler, M. E., & Dogan, A. (2012). Laser microdissection and mass spectrometry-based proteomics aids the diagnosis and typing of renal amyloidosis. *Kidney International*, *82*(2), 226–234. https://doi.org/10.1038/ki.2012.108
12. Vrana, J. A., Gamez, J. D., Madden, B. J., Theis, J. D., Bergen, H. R., & Dogan, A. (2009). Classification of amyloidosis by laser microdissection and mass spectrometry-based proteomic analysis in clinical biopsy specimens. *Blood*, *114*(24), 4957–4959. doi: blood-2009-07-230722 [pii];10.1182/blood-2009-07-230722 [doi] https://doi.org/10.1182/blood-2009-07-230722
13. Dogan, A. (2017). Amyloidosis: Insights from proteomics. *Annual Review of Pathology: Mechanisms of Disease*, *12*, 277–304. https://doi.org/10.1146/annurev-pathol-052016-100200
14. Sethi, S., Fervenza, F. C., Zhang, Y., Zand, L., Vrana, J. A., Nasr, S. H., Theis, J. D., Dogan, A., & Smith, R. J. H. (2012). C3 glomerulonephritis: Clinicopathological findings, complement abnormalities, glomerular proteomic profile, treatment, and follow-up. *Kidney International*, *82*(4), 465–473. https://doi.org/10.1038/ki.2012.212
15. Sethi, S., Zand, L., De Vriese, A. S., Specks, U., Vrana, J. A., Kanwar, S., Kurtin, P., Theis, J. D., Angioi, A., Cornell, L., & Fervenza, F. C. (2017). Complement activation in pauci-immune necrotizing and crescentic glomerulonephritis: Results of a proteomic analysis. *Nephrology, Dialysis, Transplantation*, *32*(suppl_1), i139-i145. https://doi.org/10.1093/ndt/gfw299
16. Aoki, M., Kang, D., Katayama, A., Kuwahara, N., Nagasaka, S., Endo, Y., Terasaki, M., Kunugi, S., Terasaki, Y., & Shimizu, A. (2018). Optimal conditions and the advantages of using laser microdissection and liquid chromatography tandem mass spectrometry for diagnosing renal amyloidosis. *Clinical and Experimental Nephrology*, *22*(4), 871–880. https://doi.org/10.1007/s10157-018-1533-y
17. Seeley, E. H., Oppenheimer, S. R., Mi, D., Chaurand, P., & Caprioli, R. M. (2008). Enhancement of protein sensitivity for MALDI imaging mass spectrometry after chemical treatment of tissue sections. *Journal of the American Society for Mass Spectrometry*, *19*(8), 1069–1077. doi: S1044-0305(08)00227-4 [pii];10.1016/j.jasms.2008.03.016 [doi] https://doi.org/10.1016/j.jasms.2008.03.016
18. Gagnon, H., Franck, J., Wisztorski, M., Day, R., Fournier, I., & Salzet, M. (2012). Targeted mass spectrometry imaging: Specific targeting mass spectrometry imaging technologies from history to perspective. *Progress in Histochemistry and Cytochemistry*, *47*(3), 133–174. https://doi.org/10.1016/j.proghi.2012.08.002
19. Goodwin, R. J. A., Pennington, S. R., & Pitt, A. R. (2008). Protein and peptides in pictures: Imaging with MALDI mass spectrometry. *Proteomics*, *8*(18), 3785–3800. https://doi.org/10.1002/pmic.200800320
20. Jones, E. A., Shyti, R., Van Zeijl, R. J. M., Van Heiningen, S. H., Ferrari, M. D., Deelder, A. M., Tolner, E. A., Van Den Maagdenberg, A. M. J. M., & Mcdonnell, L. A. (2012). Imaging mass spectrometry to visualize biomolecule distributions in mouse brain tissue following hemispheric cortical spreading depression. *Journal of Proteomics*, *75*(16), 5027–5035. https://doi.org/10.1016/j.jprot.2012.06.025
21. Winter, M., Tholey, A., Krüger, S., Schmidt, H., & Röcken, C. (2015). MALDI-mass spectrometry imaging identifies vitronectin as a common constituent of amyloid deposits. *Journal of Histochemistry and Cytochemistry*, *63*(10), 772–779. https://doi.org/10.1369/0022155415595264
22. Casadonte, R., Kriegsmann, M., Deininger, S.-O., Amann, K., Paape, R., Belau, E., Suckau, D., Fuchser, J., Beckmann, J., Becker, M., & Kriegsmann, J. (2015). Imaging mass spectrometry analysis of renal amyloidosis biopsies reveals protein co-localization with amyloid deposits. *Analytical and Bioanalytical Chemistry*, *407*(18), 5323–5331. https://doi.org/10.1007/s00216-015-8689-z
23. Pontil, M., & Verri, A. (1998). Properties of support vector machines. *Neural Computation*, *10*(4), 955–974. https://doi.org/10.1162/089976698300017575
24. Winter, M., Tholey, A., Kristen, A., & Röcken, C. (2017). MALDI mass spectrometry imaging: A novel tool for the identification and classification of amyloidosis. *Proteomics*, *17*(22), 1700236. https://doi.org/10.1002/pmic.201700236
25. Baumgart, J.-V., Stuhlmann-Laeisz, C., Hegenbart, U., Nattenmüller, J., Schönland, S., Krüger, S., Behrens, H.-M., & Röcken, C. (2018). Local vs. systemic pulmonary amyloidosis—Impact on diagnostics and clinical management. *Virchows Archiv*, *473*(5), 627–637. https://doi.org/10.1007/s00428-018-2442-x
26. Gioeva, Z., Urban, P., Rüdiger Meliss, R., Haag, J., Axmann, H.-D., Siebert, F., Becker, K., Radtke, H.-G., & Röcken, C. (2013). ATTR amyloid in the carpal tunnel ligament is frequently of wildtype transthyretin origin. *Amyloid*, *20*(1), 1–6. https://doi.org/10.3109/13506129.2012.750604
27. Yumlu, S., Barany, R., Eriksson, M., & Röcken, C. (2009). Localized insulin-derived amyloidosis in patients with diabetes mellitus: A case report. *Human Pathology*, *40*(11), 1655–1660. doi: S0046-8177(09)00167-1 [pii];10.1016/j.humpath.2009.02.019 [doi] https://doi.org/10.1016/j.humpath.2009.02.019
28. Doellinger, J., Schneider, A., Hoeller, M., & Lasch, P. (2020). Sample preparation by easy extraction and digestion (SPEED)— A universal, rapid, and detergent-free protocol for proteomics based on acid extraction. *Molecular and Cellular Proteomics*, *19*(1), 209–222. https://doi.org/10.1074/mcp.TIR119.001616
29. Rottenaicher, G. J., Weber, B., Rührnößl, F., Kazman, P., Absmeier, R. M., Hitzenberger, M., Zacharias, M., & Buchner, J. (2021). Molecular mechanism of amyloidogenic mutations in hypervariable regions of antibody light chains. *Journal of Biological Chemistry*, *100334*, 100334. https://doi.org/10.1016/j.jbc.2021.100334
30. Simes, R. J. (1986). An improved Bonferroni procedure for multiple tests of significance. *Biometrika*, *73*(3), 751–754. https://doi.org/10.1093/biomet/73.3.751
31. Perez-Riverol, Y., Csordas, A., Bai, J., Bernal-Llinares, M., Hewapathirana, S., Kundu, D. J., Inuganti, A., Griss, J., Mayer, G., Eisenacher, M., Pérez, E., Uszkoreit, J., Pfeuffer, J., Sachsenberg, T., Yılmaz, Ş., Tiwary, S., Cox, J., Audain, E., Walzer, M., … Vizcaíno, J. A. (2019). The PRIDE database and related tools and resources in 2019: Improving support

for quantification data. *Nucleic Acids Research*, *47*(D1), D442-D450. https://doi.org/10.1093/nar/gky1106
32. Gjeorgjievski, M., Purohit, T., Amin, M. B., Kurtin, P. J., & Cappell, M. S. (2015). Upper gastrointestinal bleeding from gastric amyloidosis in a patient with smoldering multiple myeloma. *Case Reports in Gastrointestinal Medicine*, *2015*, 320120. https://doi.org/10.1155/2015/320120
33. Grogg, K. L., Aubry, M.-C., Vrana, J. A., Theis, J. D., & Dogan, A. (2013). Nodular pulmonary amyloidosis is characterized by localized immunoglobulin deposition and is frequently associated with an indolent B-cell lymphoproliferative disorder. *American Journal of Surgical Pathology*, *37*(3), 406–412. https://doi.org/10.1097/PAS.0b013e318272fe19
34. Kim, M. J., Mccroskey, Z., Piao, Y., Belcheva, A., Truong, L., Kurtin, P. J., & Ro, J. Y. (2018). Spheroid-type of AL amyloid deposition associated with colonic adenocarcinoma: A case report with literature review. *Pathology International*, *68*(2), 123–127. https://doi.org/10.1111/pin.12618
35. Lavatelli, F., & Vrana, J. A. (2011). Proteomic typing of amyloid deposits in systemic amyloidoses. *Amyloid*, *18*(4), 177–182. https://doi.org/10.3109/13506129.2011.630762
36. Said, S. M., Grogg, K. L., & Smyrk, T. C. (2015). Gastric amyloidosis: Clinicopathological correlations in 79 cases from a single institution. *Human Pathology*, *46*(4), 491–498. https://doi.org/10.1016/j.humpath.2014.12.009
37. Brambilla, F., Lavatelli, F., Di Silvestre, D., Valentini, V., Palladini, G., Merlini, G., & Mauri, P. (2013). Shotgun protein profile of human adipose tissue and its changes in relation to systemic amyloidoses. *Journal of Proteome Research*, *12*(12), 5642–5655. https://doi.org/10.1021/pr400583h
38. Claus, S., Meinhardt, K., Aumüller, T., Puscalau-Girtu, I., Linder, J., Haupt, C., Walther, P., Syrovets, T., Simmet, T., & Fändrich, M. (2017). Cellular mechanism of fibril formation from serum amyloid A1 protein. *EMBO Reports*, *18*(8), 1352–1366. https://doi.org/10.15252/embr.201643411
39. Ke, P. C., Zhou, R., Serpell, L. C., Riek, R., Knowles, T. P. J., Lashuel, H. A., Gazit, E., Hamley, I. W., Davis, T. P., Fändrich, M., Otzen, D. E., Chapman, M. R., Dobson, C. M., Eisenberg, D. S., & Mezzenga, R. (2020). Half a century of amyloids: Past, present and future. *Chemical Society Reviews*, *49*(15), 5473–5509. https://doi.org/10.1039/C9CS00199A
40. Stroo, E., Koopman, M., Nollen, E. A. A., & Mata-Cabana, A. (2017). cellular regulation of amyloid formation in aging and disease. *Frontiers in Neuroscience*, *11*, 64. https://doi.org/10.3389/fnins.2017.00064
41. Bergström, J., Murphy, C., Eulitz, M., Weiss, D. T., Westermark, G. T., Solomon, A., & Westermark, P. (2001). Codeposition of apolipoprotein A-IV and transthyretin in senile systemic (ATTR) amyloidosis. *Biochemical and Biophysical Research Communications*, *285*(4), 903–908. https://doi.org/10.1006/bbrc.2001.5260
42. Brambilla, F., Lavatelli, F., Di Silvestre, D., Valentini, V., Rossi, R., Palladini, G., Obici, L., Verga, L., Mauri, P., & Merlini, G. (2012). Reliable typing of systemic amyloidoses through proteomic analysis of subcutaneous adipose tissue. *Blood*, *119*(8), 1844–1847. https://doi.org/10.1182/blood-2011-07-365510
43. Gallo, G., Wisniewski, T., Choi-Miura, N. H., Ghiso, J., & Frangione, B. (1994). Potential role of apolipoprotein-E in fibrillogenesis. *Am J Pathol*, *145*, 526–530.
44. Pepys, M. B., Rademacher, T. W., Amatayakul-Chantler, S., Williams, P., Noble, G. E., Hutchinson, W. L., Hawkins, P. N., Nelson, S. R., Gallimore, J. R., & Herbert, J. (1994). Human serum amyloid P component is an invariant constituent of amyloid deposits and has a uniquely homogeneous glycostructure. *Proceedings of the National Academy of Sciences of the United States of America*, *91*, 5602–5606. https://doi.org/10.1073/pnas.91.12.5602
45. Dasari, A. K. R., Hughes, R. M., Wi, S., Hung, I., Gan, Z., Kelly, J. W., & Lim, K. H. (2019). Transthyretin aggregation pathway toward the formation of distinct cytotoxic oligomers. Distinct cytotoxic oligomers. *Science Reports*, *9*(1), 33. https://doi.org/10.1038/s41598-018-37230-1
46. Wang, L., Lashuel, H. A., Walz, T., & Colon, W. (2002). Murine apolipoprotein serum amyloid A in solution forms a hexamer containing a central channel. *Proceedings of the National Academy of Sciences of the United States of America*, *99*(25), 15947–15952. https://doi.org/10.1073/pnas.252508399
47. Westermark, G. T., Fändrich, M., Lundmark, K., & Westermark, P. (2018). Noncerebral amyloidoses: Aspects on seeding, cross-seeding, and transmission, *8*(1). https://doi.org/10.1101/cshperspect.a024323
48. Ramirez-Alvarado, M. (2012). Amyloid formation in light chain amyloidosis. *Current Topics in Medicinal Chemistry*, *12*(22), 2523–2533. https://doi.org/10.2174/1568026611212220007
49. Radamaker, L., Lin, Y.-H., Annamalai, K., Huhn, S., Hegenbart, U., Schönland, S. O., Fritz, G., Schmidt, M., & Fändrich, M. (2019). Cryo-EM structure of a light chain-derived amyloid fibril from a patient with systemic AL amyloidosis. *Nature Communications.*, *10*(1), 1103. https://doi.org/10.1038/s41467-019-09032-0
50. Stepanenko, O. V., Sulatsky, M. I., Mikhailova, E. V., Stepanenko, O. V., Kuznetsova, I. M., Turoverov, K. K., & Sulatskaya, A. I. (2021). Trypsin induced degradation of amyloid fibrils. *International Journal of Molecular Sciences*, *22*(9), 4828. https://doi.org/10.3390/ijms22094828

SUPPORTING INFORMATION

Additional supporting information may be found online https://doi.org/10.1002/prca.202000079 in the Supporting Information section at the end of the article.

How to cite this article: Schürmann, J., Gottwald, J., Rottenaicher, G, Tholey, A., & Röcken, C. (2021). MALDI mass spectrometry imaging unravels organ and amyloid-type specific peptide signatures in pulmonary and gastrointestinal amyloidosis. *Prot Clin Appl.*, *15*, e2000079. https://doi.org/10.1002/prca.202000079